Microbubbles and ultrasound increase intraventricular polyplex gene transfer to the brain

James-Kevin Y. Tan[a,b], **Binhan Pham**[a,b], **Yujin Zong**[c,d], **Camilo Perez**[a,c], **Don O. Maris**[e], **Ashton Hemphill**[a,b], **Carol Miao**[f], **Thomas J. Matula**[c], **Pierre D. Mourad**[e], **Hua Wei**[g], **Drew L. Sellers**[a,b], **Philip J. Horner**[e,*], and **Suzie H. Pun**[a,b,*]

[a]Department of Bioengineering, University of Washington, Seattle, WA 98195, USA

[b]Molecular Engineering and Sciences Institute, University of Washington, Seattle, WA 98195, USA

[c]Center for Industrial and Medical Ultrasound, University of Washington, Seattle, WA 98195, USA

[d]Department of Biomedical Engineering, Xian Jiaotong University, Xi'an, 710049, China

[e]Department of Neurological Surgery, University of Washington, Seattle, WA 98109, USA

[f]Department of Pediatrics, University of Washington, Seattle, WA 98195, USA

[g]Department of Chemistry, Lanzhou University, Lanzhou 730000 China

Abstract

Neurons in the brain can be damaged or lost from neurodegenerative disease, stroke, or traumatic injury. Although neurogenesis occurs in mammalian adult brains, the levels of natural neurogenesis are insufficient to restore function in these cases. Gene therapy has been pursued as a promising strategy to induce differentiation of neural progenitor cells into functional neurons. Non-viral vectors are a preferred method of gene transfer due to potential safety and manufacturing benefits but suffer from lower delivery efficiencies compared to viral vectors. Since the neural stem and progenitor cells reside in the subventricular zone of the brain, intraventricular injection has been used as an administration route for gene transfer to these cells. However, the choroid plexus epithelium remains an obstacle to delivery. Recently, transient disruption of the blood-brain barrier by microbubble-enhanced ultrasound has been used to successfully improve drug delivery to the brain after intravenous injection. In this work, we demonstrate that microbubble-enhanced ultrasound can similarly improve gene transfer to the subventricular zone after intraventricular injection. Microbubbles of different surface charges (neutral, slightly cationic, and cationic) were prepared, characterized by acoustic flow cytometry, and evaluated for their ability to increase the permeability of immortalized choroid plexus epithelium monolayers *in*

Corresponding authors: Suzie H. Pun, spun@uw.edu, University of Washington: Department of Bioengineering and Molecular Engineering and Sciences Institute, William H. Foege Building, Box 355061, Seattle, WA 98195, USA. Philip J. Horner, pjhorner@houstonmethodist.org, Houston Methodist Research Institute, Center for Neuroregenerative Medicine, 6670 Bertner, Ave., MSR10-112, Houston, TX 77030.

vitro. Based on these results, slightly cationic microbubbles were evaluated for microbubble and ultrasound-mediated enhancement of non-viral gene transfer *in vivo*. When coupled with our previously reported gene delivery vehicles, the slightly cationic microbubbles significantly increased ultrasound-mediated transfection of the murine brain when compared to commercially available Definity® microbubbles. Temporary disruption of the choroid plexus by microbubble-enhanced ultrasound is therefore a viable way of enhancing gene delivery to the brain and merits further research.

Graphical Abstract
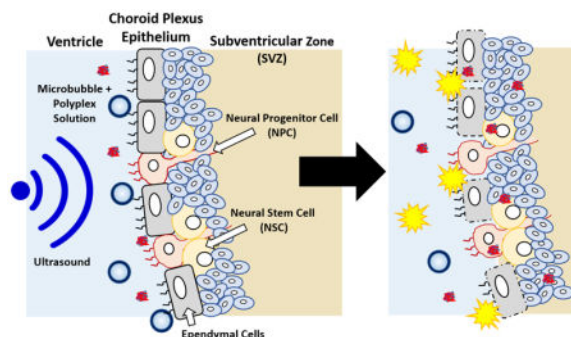
Keywords

gene delivery; microbubble; polyplex; ultrasound; *in vivo*; choroid plexus epithelium

1. Introduction

Neurological diseases or injuries such as ischemic stroke can induce a natural neurogenesis response that includes proliferation of neural progenitor cells (NPCs) and neural stem cells (NSCs) in the subventricular zone (SVZ), angiogenesis, and migration of NPCs and NSCs toward the injury site, where they differentiate and mature [1–3]. However, only a limited fraction of these cells differentiate into functional, mature neurons [4,5]. Gene delivery strategies that encourage NPC and NSC differentiation into neurons can potentially improve the recovery of lost neuron populations and help restore function [6]. For example, the delivery of genes encoding for fibroblast growth factor-2, epidermal growth factor, insulin growth factor-1, and vascular endothelial growth factor have been shown to increase neuron regeneration after ischemic stroke or delay the progression of amyotrophic lateral sclerosis in mice, rats, and gerbils [7–10]. *In vivo* gene delivery to NPCs and NSCs in the stem cell niche of the brain is therefore a promising strategy to enhance neurogenesis and offers several advantages over protein delivery and stem cell transplant therapy such as a more sustained expression that localizes in a migrating cell population and a more straightforward clinical translation, respectively. Nevertheless, there still remains a significant need for effective methods for gene transfer to the NPC and NSC populations in the brain.

Previously, our group designed and synthesized a polymeric carrier that demonstrated successful gene transfer to the subventricular zone [11]. This copolymer, PCL-SS-p[(GMA-TEPA)-*s*-OEGMA], consists of a block of poly(ε-caprolactone) (PCL) connected by a

reducible disulfide to a statistical copolymer of tetraethylenepentamine (TEPA)-decorated poly(glycidyl methacrylate) (GMA) and oligo(ethylene glycol) monomethyl ether methacrylate (OEGMA). The cationic TEPA groups of the polymer bind to and condense nucleic acids to form polyplexes while the hydrophobic PCL and hydrophilic OEGMA provide extracellular stability. After polyplex internalization, the TEPA groups contribute to endosomal escape by the proton sponge effect and the internal disulfide bond can be reduced by cytosolic glutathione facilitating polyplex destabilization and nucleic acid release. These PCL-SS-p[(GMA-TEPA)-*s*-OEGMA] polyplexes were shown to have diameters less than 200 nm and delivered nucleic acids to mouse brains *in vivo* after intraventricular injection [11]. However, gene transfer was limited to a few cell layers adjacent to the ventricular surface [12].

Along the cavities of the ventricles lie the choroid plexus barrier, comprised of choroid plexus epithelium cells that secrete cerebrospinal fluid [13,14]. These ependymal cells are held together by tight junctions and prevent materials from entering the brain parenchyma after intraventricular injection [15]. For example, both small molecules such as 1,3-bis(2-chloroethyl-1-nitroso-urea) and macromolecules such as brain-derived neurotrophic factor have limited permeation through the choroid plexus and only 1% diffuse 1 mm into the barrier [13]. We therefore hypothesized that the ependymal cells of the choroid plexus epithelium act as a significant barrier to gene transfer in the subventricular zone after intraventricular injection.

To transiently disrupt cell barriers, microbubbles (MBs), or gas-filled microspheres, have been coupled with ultrasound (US) as a method to permeabilize cell membranes and break up tight junctions, thus allowing for enhanced penetration of materials [16–18]. This process, called sonoporation, creates micropores as MBs act as local enhancers of acoustic energy and cavitate causing local shear flow, microstreams, and microjets [16,19,20]. The micropores can be spatially and temporally controlled by varying the parameters and location of US. Intravenous injections of MBs with transcranial US have been applied to the CNS to temporarily disrupt the blood-brain barrier and allow for the permeation of macromolecules such as immunoglobulinG and 70 kDa dextran into the brain [21–28]. However, to our knowledge, sonoporation of the choroid plexus epithelium as a way to enhance permeation of materials into the brain parenchyma has yet to be reported.

Herein, we investigate MB-enhanced US as a method to increase gene transfer to the brain parenchyma after intraventricular injection. Custom, lipid-based MBs of neutral, slightly cationic, and cationic charge were formulated and compared to commercially available Definity® (Def) MBs. Neutral and slightly cationic MBs, but not Definity MBs, were able to increase the permeability of cell monolayers *in vitro*. Furthermore, co-delivery of SCat MBs with polyplexes increased *in vivo* gene transfer to the brain. Sonoporation of the choroid plexus is a viable method to increase gene transfection after intraventricular injection. Further investigation may allow for the effective permeation of gene delivery vehicles through the choroid plexus into the SVZ to augment transfection of NPCs and NSCs and drive neuron differentiation and neurogenesis.

2. Materials and methods

2.1 Materials

Lipids were purchased from Avanti Polar Lipids, Inc. (Alabaster, AL) and perfluorobutane (PFB) was purchased from Synquest Laboratories (Alachua, FL). Definity® MBs and a Vialmix® machine were purchased from Lantheus Medical Imaging (N. Billerica, MA); Optison® MBs were from GE Healthcare (Chicago, IL). The Z310 choroid plexus cell line was a generous gift from Dr. Wei Zheng at Purdue University. Tissue culture reagents and bicinchoninic acid (BCA) protein quantification assay kit were purchased from Thermo Fisher Scientific (Waltham, MA). The 70 kDa Texas Red-dextran was purchased from Life Technologies (Carlsbad, CA) while the 5 kDa FITC-PEG was purchased from NanoCS (New York, NY). The pCMV-Luc2 plasmid was isolated using the Qiagen Plasmid Giga Kit (Hilden, Germany) while the pmaxGFP™ was from Lonza (Walkersville, MD). The luciferase expression quantification kit and MTS assay was obtained from Promega (Madison, WI).

2.2 MB formation and characterization

Custom MBs of different surface charges were formulated by mixing a total of 1 mg of different chloroform-dissolved lipids in a 2 mL tube followed by overnight drying under vacuum. Neu MBs were formulated at a 9:1 molar ratio of 1,2-distearoyl-*sn*-glycero-3-phosphocholine (DSPC) and 1,2-distearoyl-*sn*-glycero-3-phosphoethanolamine-*N*-[methoxy(polyethylene glycol)2000] (DSPE-mPEG2000), SCat MBs were formulated at a 9:1 molar ratio of DSPC and 1,2-distearoyl-*sn*-glycero-3-phosphoethanolamine-*N*-[amino(polyethylene glycol)2000] (DSPE-PEG2000-Amine), and Cat MBs were formulated at a 9:2:1 molar ratio of DSPC, DSPE-PEG2000-Amine, and 1,2-distearoyl-3-trimethylammonium-propane (DSTAP). The lipid film was rehydrated in a 1 mL solution of 10:10:80 (v/v/v) glycerol:propylene glycol:water at 67 °C. The tube headspace was filled with PFB and amalgamated with a Vialmix® machine for 45 s. The MB suspension was processed by differential centrifugation to remove micelles/free lipids and to isolate MBs with diameters less than 2 μm as previously described [29]. Definity® MBs were processed as per manufacturer's instructions. MB diameter and concentration were determined by a Beckman Coulter Multisizer 3 (Brea, CA). The zeta potential of the MBs was determined in 10 mM PBS pH 7.4 by a Malvern Zetasizer Nano ZS (Westborough, MA). Mechanical shell properties were characterized by a modified flow cytometer that had a piezoelectric ultrasound transducer coupled to the flow channel [30–32]. US was applied at 1 MHz and as the MBs flowed through the channel, instantaneous change in their size in response to acoustic energy was characterized by change in laser scattering signal that was detected by a photomultiplier tube. This data was fitted to previously reported MB models and the mechanical MB parameters were determined [33].

2.3 Synthesis of PCL-SS-p[(GMA-TEPA)-*s*-OEGMA]

The reducible 2-hydroxyethyl-2′-(bromoisobutyryl)ethyl disulfide double-head initiator (HO-SS-iBuBr) and PCL-SS-p[(GMA-TEPA)-*s*-OEGMA] were synthesized as previously reported [11]. Briefly, ring-opening polymerization (ROP) of caprolactone was performed using HO-SS-iBuBr as the initiator and Sn(Oct)$_2$ as the catalyst. Then, a one-pot atom-

transfer radical polymerization (ATRP) of GMA and OEGMA was performed using PCL_{40}-SS-iBuBr as the macroinitiator and CuCl/bpy as the catalyst. The copolymer composition and molecular weight were determined by ^{1}HNMR and gel permeation chromatography (GPC) using an Optilab-rEX and miniDAWN TREOS triple-angle static light scattering detector (Wyatt Technology, Santa Barbara CA). The GMA monomers in the polymer were reacted with excess TEPA in dimethylacetamide.

2.4 Polyplex Formation

The pCMV-Luc2 plasmid was diluted in double-distilled H_2O (ddH2O) to a concentration of 0.1 mg/mL and mixed with an equal volume of polymer (in ddH_2O) at an amine-to-phosphate (N/P) ratio = 15. The required amount of polymer was calculated by determining the polymer mass-to-charge ratio and taking into account that 1 µg of DNA contains 3 nmol of phosphate. After mixing, the polyplexes were allowed to form for 10 min at room temperature.

2.5 MB Stability

MB stability was assessed by measuring the MB concentration over time with a Multisizer 3 relative to the initial MB concentration. In a similar manner, MB stability was assessed while in the presence of polyplexes at a ratio of 1.25×10^7 MBs/µg DNA.

2.6 MB Stability Cytotoxicity

Immortalized Z310 choroid plexus cells were cultured in 10% heat-inactivated FBS, 1% penicillin-streptomycin, 40 µg/mL gentamicin, and 10 ng/mL endothelial growth factor-supplemented DMEM culture medium as previously described [34,35]. MBs (1.25×10^7) were dispensed into each well of a 96 well plate with 10,000 adhered Z310 cells. The plate was covered with an adhesive plate seal film and inverted so that MBs would rise and be in contact with the cells. After 30 min in an incubator, an MTS assay was performed to assess cell viability.

2.7 Polyplex Stability with Microbubbles

The ability of polyplexes to remain complexed in the presence of MBs was assessed by a gel retardation assay. The polyplexes (1 µg DNA, 20 µL solution, N/P = 15) were incubated with 1.25×10^7 MBs/µg DNA for 10 min. Solutions were mixed with 10% (v/v) BlueJuice™gel loading buffer (Invitrogen, Carlsbad, CA) and loaded onto a 1% agarose gel containing TAE buffer (40 mM tris-acetate, 1 mM EDTA) and 5 mg/mL ethidium bromide. The gel was electrophoresed at 100 V for 40 min. The plasmid DNA was then visualized using a Kodak (Rochester, NY) UV transilluminator (laser-excited fluorescence gel scanner).

2.8 MBs turbidity assay

In a water bath, MBs were sonicated by a diagnostic Sonosite MicroMaxx® machine (Bothell, WA) with a P17 transducer (center frequency: 3 MHz, imaging modality: general, mechanical index: 0.8, phased array, pen mode, 4.7 cm depth). The turbidity of the MB suspension was assessed by measuring the absorbance at 900 nm, relative to unsonicated MBs.

2.9 *In vitro* Z310 permeability studies

Z310 cells were seeded in Transwell® permeable supports at 10,000 cells/transwell and were allowed to grow in a 24 well plate for 3 days. Monolayer formation was verified by transepithelial electrical resistance measurements with an EVOM instrument (World Precision Instruments, Sarasota, FL). For permeability studies, transwells were washed, submerged, and inverted into an OptiMEM® bath. Underneath the bath, a P17 transducer was pointed upwards towards the transwell and was controlled by a SonoSite MicroMaxx® machine. MBs (2.5×10^7) were pipetted in the transwell space between the cells and the glass bath container and US was applied for 15 s. Afterwards, the transwell was removed from the bath, washed with OptiMEM®, and placed in a well plate. An OptiMEM® solution of 0.02 mM 5 kDa FITC-PEG and 0.02 mM 70 kDa Texas-Red dextran was added to each transwell. After 4 hour incubation, samples were taken from the bottom well plate and the fluorescence was measured (FITC ex: 492 nm, em: 518 nm; Texas Red: ex: 595 nm, em: 615 nm). Permeability was expressed as a percentage of the average control value. In addition, Z310 cells were analyzed by flow cytometry to measure fluorescence uptake. Z310 cells in transwells were treated with SCat MBs and US as mentioned above. The solution was replaced with 0.02 mM of 5 kDa FITC-PEG and placed in an incubator for 1 hr. The cells were washed, trypsinized, collected, and washed before flow cytometry analysis with a MACSQuant (Miltenyi, Bergisch Gladbach, Germany) flow cytometer. Analysis was performed with FlowJo analysis software (Tree Star, Ashland, Oregon).

2.10 *In vivo* MB, US, and polyplex transfection

All animal procedures were completed using protocols approved by the Institutional Animal Care and Use Committee at the University of Washington. Luciferase or GFP reporter polyplexes were prepared in 5% glucose using 2.5 μg of DNA in 10 μL total volume at an N/P = 15 as previously described [36]. Adult (8–9 weeks) female C57BL/6J mice (Jackson Laboratories) were anesthetized by an intraperitoneal injection of Avertin. A 1 mm diameter craniotomy was made on the right side of the skull using a dental drill and 10 μL of polyplex or polyplex/MB suspension at 1.25×10^7 MBs/μg DNA (n = 6 or 9 per group) was stereotaxically injected at 1 mm lateral, 0.5 mm caudal to bregma, and 1.9 mm depth from the dura using a 33 gauge 10 μL Hamilton syringe. The injection was made over 2.5 minutes and the syringe was kept in place for 2 minutes after injection to prevent backflow. Afterwards, a P17 transducer was held to the mouse skull and US was applied for 1 min with a SonoSite MicroMaxx® machine.

2.11 Luciferase expression analysis

Brains were harvested from mice 48 hours post injection and separated into three sections: hindbrain, left brain, and right brain. Tissues were collected in 1X reporter lysis buffer (RLB, Promega Corp., Madison, WI) with 1X EDTA-free Roche's Complete Protease Inhibitor Cocktail (Roche, Nutley, NJ) and three freeze-thaw cycles were performed in liquid nitrogen. Tissues were mechanically homogenized and cell debris were pelleted at 15,000 *g* for 15 min at 4 °C. The lysates were collected and analyzed by a luciferase assay kit (integration time = 1 s) and by the BCA assay to normalize luciferase expression by protein content.

2.12 Immunohistochemistry and confocal microscopy

Polyplexes formulated with pmaxGFP™ were administered by intraventricular injection to mice as described above. Two days post-injection, mice were euthanized and perfused intracardially with 0.9% saline followed by 4% paraformaldehyde in 0.1 M phosphate buffer. After perfusion and fixation, the brains were excised and equilibrated to 30% sucrose in phosphate buffer. Brains were embedded in OCT and sectioned into 40 um-thick coronal slices. For immunofluorescent labeling, slides were rinsed with PBS and blocked in PBS, 0.3% TritonX-100, 2% bovine serum albumin (BSA) for 1 hour. Primary antibodies (goat anti-Sox2 (1:250), Santa Cruz Biotechnology; chicken anti-vimentin (1:250), EMD Millipore) were applied to the tissue sections in PBS, 0.3% TritonX-100, 2% BSA overnight at 4 °C. Sections were rinsed three times for 20 minutes in TBS, 0.1% Tween 20 and species appropriate secondary antibodies conjugated with fluorophore were incubated in PBS, 0.1% Tween 20, and 2% donkey serum for 2 hours. Sections were rinsed three times for 20 minutes in TBS-Tween, with the last rinse containing the nuclear marker, 4′,6-diamidino-2-phenylindole (DAPI; 1:1000). Sections were then mounted onto glass slides, sealed and cover-slipped with gelvatol, and imaged using a confocal microscope.

2.13 Statistical Analysis

All statistical analyses were performed using a two-tailed Student's t-test with unequal variance.

3. Results and Discussion

MB-enhanced US has been used to disrupt the blood-brain barrier to facilitate the penetration of immunoglobulinG, dextrans, and viruses [23,37–39]. Herein, we focus on MB sonoporation to temporarily disrupt the choroid plexus barrier after intraventricular injection. Direct injection allows for close proximity to the neuron stem cell niche of the subventricular zone (SVZ) while keeping the BBB intact. In this paper, three custom MBs were developed, characterized, and evaluated *in vitro* and *in vivo* as a non-viral gene delivery system that combines physical and chemical delivery methods for gene transfer into the SVZ.

3.1 Microbubble and polyplex characterization

Three custom, lipid-based microbubble (MB) formulations with different surface charges, Neutral (Neu), Slightly Cationic (SCat), and Cationic (Cat), were prepared and compared to commercially available, neutrally charged Definity® (Def) MBs and negatively charged Optison® (Opt) MBs. Different surface charges of the custom MBs were obtained by varying the lipid compositions and the chemical termini of the lipids (Table 1).

Neutral microbubbles were formulated with 90% DSPC and 10% DSPE-mPEG2000. The cationic charge in SCat MBs was obtained by replacing DSPE-mPEG with an amine-terminated PEG, DSPE-PEG-Amine. While most positively charged MBs are formulated by replacing 20% of the DSPC lipids with cationic DSTAP lipids; here, switching the end chemistry of the PEGylated lipid provided another way to change MB surface charge. A higher cationic surface charge with the Cat MBs was obtained by using both DSPE-PEG-

Amine and cationic lipid DSTAP. The custom MBs were prepared from rehydrated lipid films with perfluorobutane using a Vialmix® amalgamator. All MBs, including the commercially available Def and Opt MBs, were similar in size (~1 μm) and concentration (~10^{10} MBs/mL) to MBs of other reports [40,41] with expected surface zeta potential values (Table 2).

The DNA condensing copolymer, PCL-SS-p[(GMA-TEPA)-s-OEGMA], was synthesized and formed polyplexes with DNA at N/P = 15 as previously described [11]. As an initial study, polyplexes were incubated with the different types of MBs to test for visible aggregation. No precipitation was observed upon addition of Neu, SCat, Cat, and Def MBs with cationic polyplexes. Conversely, mixing with the Opt MBs resulted in rapid aggregation and precipitation likely due to the strong electrostatic interactions between the anionic shell of the albumin-coated Opt MBs and the cationic polyplexes. Therefore, we decided to move forward with the other types of MBs and exclude Opt MBs from further investigation.

Next, the MBs were characterized by acoustic flow cytometry and MB modeling was utilized to determine the mechanical shell properties of the MBs [30–32] (Figure 1). An ultrasonic transducer was coupled to a conventional flow cytometer and MBs were sonicated as they pass through the laser interrogation region of the flow channel. In response to the acoustic energy, the MBs undergo an instantaneous change in size which was detected by a change in laser scattering. The radial dynamics were fitted to a Marmottant MB model to extract the shell elastic modulus (χ) and the shell dilatational viscosity (κ_S).

The shell elastic modulus, or the stiffness of the MB shell, was similar for all three custom MB formulations, ranging from around 0.05 to 0.10 N/m (Figure 1A). The elastic modulus was relatively independent of MB size as consistent with other lipid MBs like Def MBs [30–32]. In contrast, the Def MBs had an order of magnitude higher shell elastic modulus, suggesting a possible higher cavitation threshold [42,43]. The shell dilatational viscosity, or compressibility of the MB, increased as a function of MB size and ranged from 1.04×10^{-9} to 7.22×10^{-9}, 2.24×10^{-9} to 1.13×10^{-8}, 2.27×10^{-9} to 8.10×10^{-9}, and 4.53×10^{-10} to 5.34×10^{-9} kg/s for the Neu, SCat, Cat, and Def MBs, respectively (Figure 1B). This suggests that there is a size dependent and thus frequency dependent effect of the viscosity as consistent with other lipid-shelled bubbles [31,33].

The stability of the MB formulations in solution was evaluated by measuring the MB concentration over time relative to initial concentration by a Multisizer 3 (Figure 2A). Microbubble concentrations decreased over the first 2 hours to nearly 50% of initial values, but then remained relatively stable over the time course of the experiment (300 min). In addition, the stability of the MB formulations in the presence of polyplexes was also evaluated (**Error! Reference source not found.**). MBs in the presence of polyplexes had a similar rate of disappearance to MBs without any polyplexes. In addition, polyplex stability in the presence of MBs was tested by a gel retardation assay (**Error! Reference source not found.**). The MBs did not affect polyplex stability and DNA remained complexed with polymer at N/P = 15.

MB cytotoxicity was assessed by incubating MBs with HeLa cells for 30 min and performing an MTS assay (**Error! Reference source not found.**). The MBs exhibited minimal cytotoxicity as the relative cell viability across all MB types was greater than 95%.

Next, we monitored MB destruction in response to US from a diagnostic Sonosite Micromaxx® US machine. The Def MBs are more elastic than the custom MBs, which can lead to more dampening under US, thus raising the inertial cavitation threshold [42,44]. This was tested by sonicating the MBs and assessing MB intactness by measuring turbidity of the solution (Figure 2B). The SCat MBs easily cavitated as half of the initial MB absorbance was lost within 1 min of sonication and only about 20% remained after 5 min of sonication. The Neu MBs were a little more robust under these US conditions and about 40% of the MB absorbance remained after 5 min of sonication. The Cat and Def MBs did not cavitate as well under these US conditions. After 5 min of sonication, about 80% of the Cat MB absorbance remained while the absorbance of the Def MBs remained relatively unchanged over the 5 min of US sonication. The Def MBs seem to have a higher cavitation threshold under these US conditions, consistent with the higher shell elastic modulus shown in Figure 1A.

3.2 *In vitro* Z310 permeability studies

The ability to sonoporate cell layers was assessed by monitoring choroid plexus monolayer permeability to hydrophilic tracer polymers of dextran (70 kDa) and PEG (5 kDa) (Figure 3A). Z310 choroid plexus epithelium cells were allowed to grow as monolayers in transwells as confirmed by transepithelial electrical resistance measurements ($+25\ \Omega$ relative to blank transwells, data not shown). Microbubbles were then added to inverted cultures to allow for contact between floating MBs and cell layers and US from a Sonosite Micromaxx® applied for 15 sec with a P17 transducer. The transwells were then transferred back to culture chambers and tracers (70 kDa Texas-Red dextran and 5 kDa FITC-PEG) added to the top compartment. Permeability to tracers was determined after sonoporation by custom MBs or by commercially available Def MBs (Figure 3B and **Error! Reference source not found.**).

Monolayer permeability was unaffected by either US treatment alone or treatment with Def, Neu, or SCat MBs in the absence of ultrasound. A slight increase in permeability was observed with cationic MB treatment alone. Cationic lipids have been shown to destabilize cell membranes and cause toxicity which may explain the slight increase in permeability without US [45,46]. With US, the Def MBs did not show an increase in sonoporation, possibly due to the higher inertial cavitation threshold afforded by the more elastic nature of the Def lipid shell and limited cavitation under these US conditions (Figure 1A and Figure 2B) [42,44]. Conversely, the custom MBs were better able to undergo inertial cavitation, sonoporate Z310 monolayers, and increase Z310 monolayer permeability. When US was applied to the Neu or SCat MB groups, Z310 monolayer permeability doubled and was statistically significant ($P < 0.05$) when compared to Cells, US, or respective MB only groups (Figure 3B and **Error! Reference source not found.**). More severe MB cavitation and collapse, as seen with the SCat and Neu MBs (Figure 2B), has been the most effective in generating membrane disruption and was linked to greater rates of membrane poration than when MBs undergo stable cavitation, coalescence, or translation [47,48]. In fact, greater US

parameters such as frequency and pressure, which cause greater MB cavitation, are consistently linked to better delivery of macromolecules across in the blood-brain barrier in mice [21,22]. On the other hand, more subtle sonoporation, such as those at low pressures, are more closely linked to MBs interacting and "massaging" the cell membrane, causing increased endocytosis [48,49]. The ability of MBs to undergo inertial cavitation at these US conditions seem to be imperative in increasing the permeability of the Z310 monolayers.

The SCat MBs may have had the highest sonoporation and increase in permeability by being the most sensitive to cavitation under these US conditions (Figure 2B) and by closely interacting with negatively charged cell membranes by electrostatic interactions. Since the impact of MB cavitation rapidly reduces with increasing distance between the MB and cell membrane [20], a higher sonoporation is achieved by minimizing the distance between the MB and the cell surface. This is consistent with the higher permeability seen after SCat MB sonoporation over Neu MB sonoporation. In addition, Z310 cells were analyzed by flow cytometry to measure fluorescence uptake. Treatment with SCat MBs, US, or SCat MBs + US did not increase FITC-PEG uptake relative to cells only under these experimental conditions (**Error! Reference source not found.**). Since the SCat MBs showed the largest increase in permeability and would interact more closely with cells by electrostatic interactions with anionic membranes, they were further evaluated *in vivo* and compared to commercially available Def MBs.

3.3 *In vivo* transfection in mouse brain

To determine if choroid plexus sonoporation would increase transfection in brains, polyplex and polyplex/MB formulations with the luciferase reporter gene were intraventricularly administered into murine right brains followed by 1 min of transcranial US applied with a Sonosite MicroMaxx® with a P17 transducer. Brains were harvested two days post-administration for analysis of transgene expression by bulk luciferase assay (Figure 4).

Mice treated with polyplex alone resulted in luciferase activity ~10^4 relative light units (RLU)/mg protein in each part of the brain as consistent with our previous report [11]. Addition of either MBs or US separately to polyplexes did not significantly affect transfection efficiency. However, a 4.35-fold increase in luciferase expression was observed by a combination of polyplexes, SCat MBs, and US ($P < 0.05$). Increased permeability of the choroid plexus likely allowed enhanced penetration of the polyplexes and subsequently a higher transfection of cells in the SVZ area. This effect was not observed with Def MBs which is consistent with the low cavitation and sonoporation seen in the turbidity assay (Figure 2B) and in the *in vitro* permeability assay (Figure 3B). While current reports demonstrate the enhanced penetration of molecules like adenoviruses and dextrans across the BBB after US [21,27,38], this study suggests that MB-enhanced US can increase the permeation of larger macromolecules such as polyplexes across the choroid plexus epithelium. In the hindbrain and left brain, the SCat and Def MBs with US had little to no effect on transfection as there was no statistically significant difference in luciferase activity among all the groups (**Error! Reference source not found.**). This is consistent with other reports of BBB opening where enhanced permeation of molecules occurred only in the

region of overlap between MB and US administration and molecules were not able to diffuse to the contralateral side [27,38,50].

3.4 Distribution of transfected cells in mouse brain

To determine the types of cells transfected after intraventricular injection, polyplexes were formed with a green fluorescence protein (GFP) reporter plasmid and brain tissues were stained for the neural progenitor/stem cell marker, Sox2; intermediate filaments found in ependymal cells, vimentin; and nuclei (Figure 5).

As seen with the luciferase expression (Figure 4), there were more transfected, GFP+-expressing cells when polyplexes were combined with SCat MBs and US than without US. SCat MBs increased GFP expression at the dorsal surface of the ventricle walls (Figure 5D & E). MB sonoporation was able to increase transfection and more GFP+ cells are found throughout the layer of the SVZ (Figure 5E) than in the brains receiving MB treatment only (Figure 5B). In the ventricle walls, significantly more GFP expression is seen in brains treated with MBs and US as evidenced by the GFP channel pictures (Figure 5C & F). Even at the most ventral side, away from the injection site, there was more transfection and GFP expression upon the addition of US. In fact, propelling MBs toward the cell surface has been shown to cause pore formation and cause an influx of molecules into the cell [49]. Since US was applied to top of the skull towards the ventral side, it is likely that some of the MBs were propelled towards the ventral walls and caused permeation of cell membranes allowing for more polyplex uptake and increased transfection. Overall, the confocal images confirm the increased number of transfected cells after MB and US treatment and support the results in the luciferase analysis (Figure 4).

4. Conclusions

In this work, three MBs (Neu, SCat, and Cat) of different surface charge were formulated and compared to commercially available Def MBs. We investigated the ability of US-treated MBs to enhance the delivery of our previously-reported polyplexes into the SVZ to increase the transfection of NPCs, NSCs, and other cells. SCat MBs best sonoporated cultured choroid plexus monolayers and caused the greatest increase in permeability. These MBs and polyplexes were injected into the ventricles of mice and US was applied to sonoporate the choroid plexus barrier to the SVZ. The SCat MBs increased transfection *in vivo* better than the commercially available Def MBs or polyplexes alone. MB disruption of the choroid plexus epithelium is a viable strategy to enhance the penetration of polyplexes into the brain and merits further research.

Supplementary Material

Refer to Web version on PubMed Central for supplementary material.

Acknowledgments

References

1. Sawada M, Sawamoto K. Mechanisms of Neurogenesis in the Normal and Injured Adult Brain. Keio J Med. 2013; 62:13–28. DOI: 10.2302/kjm.2012-0005-RE [PubMed: 23563788]

2. Zheng W, ZhuGe Q, Zhong M, Chen G, Shao B, Wang H, et al. Neurogenesis in adult human brain after traumatic brain injury. J Neurotrauma. 2013; 30:1872–80. DOI: 10.1089/neu.2010.1579 [PubMed: 21275797]

3. Saha B, Peron S, Murray K, Jaber M, Gaillard A. Cortical lesion stimulates adult subventricular zone neural progenitor cell proliferation and migration to the site of injury. Stem Cell Res. 2013; 11:965–77. DOI: 10.1016/j.scr.2013.06.006 [PubMed: 23900166]

4. Parent JM, Vexler ZS, Gong C, Derugin N, Ferriero DM. Rat forebrain neurogenesis and striatal neuron replacement after focal stroke. Ann Neurol. 2002; 52:802–13. DOI: 10.1002/ana.10393 [PubMed: 12447935]

5. Arvidsson A, Collin T, Kirik D, Kokaia Z, Lindvall O. Neuronal replacement from endogenous precursors in the adult brain after stroke. Nat Med. 2002; 8:963–70. DOI: 10.1038/nm747 [PubMed: 12161747]

6. Goldman S. Stem and progenitor cell-based therapy of the human central nervous system. Nat Biotechnol. 2005; 23:862–71. DOI: 10.1038/nbt1119 [PubMed: 16003375]

7. Matsuoka N, Nozaki K, Takagi Y, Nishimura M, Hayashi J, Miyatake SI, et al. Adenovirus-mediated gene transfer of fibroblast growth factor-2 increases BrdU-positive cells after forebrain ischemia in gerbils. Stroke. 2003; 34:1519–25. DOI: 10.1161/01.STR.0000070840.56414.3B [PubMed: 12730553]

8. Sugiura S, Kitagawa K, Tanaka S, Todo K, Omura-Matsuoka E, Sasaki T, et al. Adenovirus-mediated gene transfer of heparin-binding epidermal growth factor-like growth factor enhances neurogenesis and angiogenesis after focal cerebral ischemia in rats. Stroke. 2005; 36:859–64. DOI: 10.1161/01.STR.0000158905.22871.95 [PubMed: 15746462]

9. Kaspar BK, Lladó J, Sherkat N, Rothstein JD, Gage FH. Retrograde viral delivery of IGF-1 prolongs survival in a mouse ALS model. Science. 2003; 301:839–42. DOI: 10.1126/science.1086137 [PubMed: 12907804]

10. Dodge JC, Treleaven CM, Fidler Ja, Hester M, Haidet A, Handy C, et al. AAV4-mediated expression of IGF-1 and VEGF within cellular components of the ventricular system improves survival outcome in familial ALS mice. Mol Ther. 2010; 18:2075–84. DOI: 10.1038/mt.2010.206 [PubMed: 20859261]

11. Wei H, Volpatti LR, Sellers DL, Maris DO, Andrews IW, Hemphill AS, et al. Dual responsive, stabilized nanoparticles for efficient in vivo plasmid delivery. Angew Chem Int Ed Engl. 2013; 52:5377–81. DOI: 10.1002/anie.201301896 [PubMed: 23592572]

12. Choi JL, Tan JY, Sellers DL, Wei H, Horner PJ, Pun SH. Guanidinylated block copolymers for gene transfer: A comparison with amine-based materials for in vitro and in vivo gene transfer efficiency. Biomaterials. 2015; 54:87–96. DOI: 10.1016/j.biomaterials.2015.03.008 [PubMed: 25907042]

13. Pardridge WM. Drug transport in brain via the cerebrospinal fluid. Fluids Barriers CNS. 2011; 8:7.doi: 10.1186/2045-8118-8-7 [PubMed: 21349155]

14. Chodobski A, Szmydynger-chodobska J. Choroid plexus: target for polypeptides and site of their synthesis. Microsc Res Tech. 2001; 52:65–82. [accessed January 20, 2014] http://onlinelibrary.wiley.com/. DOI: 10.1002/1097-0029(20010101)52:1%3C65::AID-JEMT9%3E3.0.CO;2-4/abstract [PubMed: 11135450]

15. Mortazavi MM, Griessenauer CJ, Adeeb N, Deep A, Shahripour RB, Loukas M, et al. The choroid plexus: A comprehensive review of its history, anatomy, function, histology, embryology, and surgical considerations. Child's Nerv Syst. 2014; 30:205–214. DOI: 10.1007/s00381-013-2326-y [PubMed: 24287511]

16. Panje CM, Wang DS, Willmann JK. Ultrasound and microbubble-mediated gene delivery in cancer: progress and perspectives. Invest Radiol. 2013; 48:755–69. DOI: 10.1097/RLI. 0b013e3182982cc1 [PubMed: 23697924]

17. Rychak JJ, Klibanov AL. Nucleic acid delivery with microbubbles and ultrasound. Adv Drug Deliv Rev. 2014; 72:82–93. DOI: 10.1016/j.addr.2014.01.009 [PubMed: 24486388]

18. Meairs S, Alonso A. Ultrasound, microbubbles and the blood-brain barrier. Prog Biophys Mol Biol. 2007; 93:354–62. DOI: 10.1016/j.pbiomolbio.2006.07.019 [PubMed: 16959303]

19. Greenleaf W, Bolander M. Artificial cavitation nuclei significantly enhance acoustically induced cell transfection. Ultrasound Med. 1998; 24:587–595. [accessed November 3, 2014] http:// www.sciencedirect.com/science/article/pii/S0301562998000039.

20. Zhou Y, Yang K, Cui J, Ye J, Deng C. Controlled permeation of cell membrane by single bubble acoustic cavitation. J Control Release. 2012; 157:103–111. DOI: 10.1016/j.jconrel. 2011.09.068.Controlled [PubMed: 21945682]

21. Choi JJ, Selert K, Gao Z, Samiotaki G, Baseri B, Konofagou EE. Noninvasive and localized blood-brain barrier disruption using focused ultrasound can be achieved at short pulse lengths and low pulse repetition frequencies. J Cereb Blood Flow Metab. 2011; 31:725–37. DOI: 10.1038/jcbfm. 2010.155 [PubMed: 20842160]

22. Choi JJ, Pernot M, Small Sa, Konofagou EE. Noninvasive, transcranial and localized opening of the blood-brain barrier using focused ultrasound in mice. Ultrasound Med Biol. 2007; 33:95–104. DOI: 10.1016/j.ultrasmedbio.2006.07.018 [PubMed: 17189051]

23. Choi JJ, Wang S, Tung YS, Morrison B, Konofagou EE. Molecules of various pharmacologically-relevant sizes can cross the ultrasound-induced blood-brain barrier opening in vivo. Ultrasound Med Biol. 2010; 36:58–67. DOI: 10.1016/j.ultrasmedbio.2009.08.006 [PubMed: 19900750]

24. Wang S, Samiotaki G, Olumolade O, Feshitan Ja, Konofagou EE. Microbubble type and distribution dependence of focused ultrasound-induced blood-brain barrier opening. Ultrasound Med Biol. 2014; 40:130–7. DOI: 10.1016/j.ultrasmedbio.2013.09.015 [PubMed: 24239362]

25. Xie F, Boska MD, Lof J, Uberti MG, Tsutsui JM, Porter TR. Effects of transcranial ultrasound and intravenous microbubbles on blood brain barrier permeability in a large animal model. Ultrasound Med Biol. 2008; 34:2028–34. DOI: 10.1016/j.ultrasmedbio.2008.05.004 [PubMed: 18692294]

26. McDannold N, Arvanitis CD, Vykhodtseva N, Livingstone MS. Temporary disruption of the blood-brain barrier by use of ultrasound and microbubbles: safety and efficacy evaluation in rhesus macaques. Cancer Res. 2012; 72:3652–63. DOI: 10.1158/0008-5472.CAN-12-0128 [PubMed: 22552291]

27. Sheikov N, McDannold N, Vykhodtseva N, Jolesz F, Hynynen K. Cellular mechanisms of the blood-brain barrier opening induced by ultrasound in presence of microbubbles. Ultrasound Med Biol. 2004; 30:979–89. DOI: 10.1016/j.ultrasmedbio.2004.04.010 [PubMed: 15313330]

28. Meairs S, Alonso A, Fatar M, Kern R, Hennerici M. Microbubbles traversing the blood-brain barrier for imaging and therapy. Med Biol Eng Comput. 2009; 47:839–49. DOI: 10.1007/ s11517-009-0468-6 [PubMed: 19283421]

29. Feshitan, Ja; Chen, CC.; Kwan, JJ.; Borden, Ma. Microbubble size isolation by differential centrifugation. J Colloid Interface Sci. 2009; 329:316–24. DOI: 10.1016/j.jcis.2008.09.066 [PubMed: 18950786]

30. Matula TJ, Swalwell J, Tu J, Cui W, Chen W. Flow cytometry to characterize microbubbles 2011. IEEE Int Ultrason Symp. 2011; :156–159. DOI: 10.1109/ULTSYM.2011.0039

31. Tu J, Swalwell JE, Giraud D, Cui W, Chen W, Matula TJ. Microbubble sizing and shell characterization using flow cytometry. IEEE Trans Ultrason Ferroelectr Freq Control. 2011; 58:955–963. DOI: 10.1109/TUFFC.2011.1896 [PubMed: 21622051]

32. Cavalieri F, Best JP, Perez C, Tu J, Caruso F, Matula TJ, et al. Mechanical characterization of ultrasonically synthesized microbubble shells by flow cytometry and AFM. ACS Appl Mater Interfaces. 2013; 5:10920–10925. DOI: 10.1021/am403108y [PubMed: 24125167]

33. Doinikov, Aa; Haac, JF.; Dayton, Pa. Modeling of nonlinear viscous stress in encapsulating shells of lipid-coated contrast agent microbubbles. Ultrasonics. 2009; 49:269–275. DOI: 10.1016/j.ultras. 2008.09.007 [PubMed: 18990417]

34. Zheng W, Zhao Q. Establishment and characterization of an immortalized Z310 choroidal epithelial cell line from murine choroid plexus. Brain Res. 2002; 958:371–80. http://www.ncbi.nlm.nih.gov/pubmed/12470873. [PubMed: 12470873]

35. Shi L, Li G, Wang S, Zheng W. Use of Z310 cells as an in vitro blood–cerebrospinal fluid barrier model: Tight junction proteins and transport properties. Toxicol Vitr. 2008; 22:190–199. DOI: 10.1016/j.tiv.2007.07.007.Use

36. Tan JKY, Choi JL, Wei H, Schellinger JG, Pun SH. Reducible, dibromomaleimide-linked polymers for gene delivery. Biomater Sci. 2015; 3:112–120. DOI: 10.1039/C4BM00240G

37. Wang S, Olumolade OO, Sun T, Samiotaki G, Konofagou EE. Noninvasive, neuron-specific gene therapy can be facilitated by focused ultrasound and recombinant adeno-associated virus. Gene Ther. 2014; 22:104–110. DOI: 10.1038/gt.2014.91 [PubMed: 25354683]

38. Weber-Adrian D, Thévenot E, O'Reilly Ma, Oakden W, Akens MK, Ellens N, et al. Gene delivery to the spinal cord using MRI-guided focused ultrasound. Gene Ther. 2015; :1–10. DOI: 10.1038/gt.2015.25

39. Wu SY, Chen CC, Tung YS, Olumolade OO, Konofagou EE. Effects of the Microbubble Shell Physicochemical Properties on Ultrasound-Mediated Drug Delivery to the Brain. J Control Release. 2015; 212:30–40. DOI: 10.1016/j.jconrel.2015.06.007 [PubMed: 26065734]

40. Wang D, Panje C, Pysz M, Ramasamy P, Rosenberg J, Gambhir S, et al. Cationic versus neutral microbubbles for ultrasound-mediated gene delivery in cancer. Radiology. 2012; 264:721–732. DOI: 10.1148/radiol.12112368/-/DC1 [PubMed: 22723497]

41. Sun RR, Noble ML, Sun SS, Song S, Miao CH. Development of therapeutic microbubbles for enhancing ultrasound-mediated gene delivery. J Control Release. 2014; 182:111–20. DOI: 10.1016/j.jconrel.2014.03.002 [PubMed: 24650644]

42. Guo X, Li Q, Zhang Z, Zhang D, Tu J. Investigation on the inertial cavitation threshold and shell properties of commercialized ultrasound contrast agent microbubbles. J Acoust Soc Am. 2013; 134:1622.doi: 10.1121/1.4812887 [PubMed: 23927202]

43. Dicker S, Mleczko M, Siepmann M, Wallace N, Sunny Y, Bawiec CR, et al. Influence of Shell Composition on the Resonance Frequency of Microbubble Contrast Agents. Ultrasound Med Biol. 2013; 39:1292–1302. DOI: 10.1016/j.ultrasmedbio.2013.02.462 [PubMed: 23683409]

44. Dicker S, Mleczko M, Schmitz G, Wrenn SP. Determination of microbubble cavitation threshold pressure as function of shell chemistry. Bubble Sci Eng Technol. 2010; 2:55–64. DOI: 10.1179/1758897910Y.0000000001

45. Lv H, Zhang S, Wang B, Cui S, Yan J. Toxicity of cationic lipids and cationic polymers in gene delivery. J Control Release. 2006; 114:100–9. DOI: 10.1016/j.jconrel.2006.04.014 [PubMed: 16831482]

46. Dass CR. Oligonucleotide delivery to tumours using macromolecular carriers. Biotechnol Appl Biochem. 2004; 40:113–122. DOI: 10.1042/BA20040005 [PubMed: 15070400]

47. Fan Z, Chen D, Deng CX. Improving ultrasound gene transfection efficiency by controlling ultrasound excitation of microbubbles. J Control Release. 2013; 170:401–13. DOI: 10.1016/j.jconrel.2013.05.039 [PubMed: 23770009]

48. Delalande A, Leduc C, Midoux P, Postema M, Pichon C. Efficient Gene Delivery by Sonoporation Is Associated with Microbubble Entry into Cells and the Clathrin-Dependent Endocytosis Pathway. Ultrasound Med Biol. 2015; :1–14. DOI: 10.1016/j.ultrasmedbio.2015.03.010

49. De Cock I, Zagato E, Braeckmans K, Luan Y, De Jong N, De Smedt SC, et al. Ultrasound and microbubble mediated drug delivery: Acoustic pressure as determinant for uptake via membrane pores or endocytosis. J Control Release. 2015; 197:20–28. DOI: 10.1016/j.jconrel.2014.10.031 [PubMed: 25449801]

50. Samiotaki G, Acosta C, Wang S, Konofagou EE. Enhanced delivery and bioactivity of the neurturin neurotrophic factor through focused ultrasound — mediated blood – brain barrier opening in vivo. J Cereb Blood Flow Metab. 2015; :1–12. DOI: 10.1038/jcbfm.2014.236 [PubMed: 25352045]
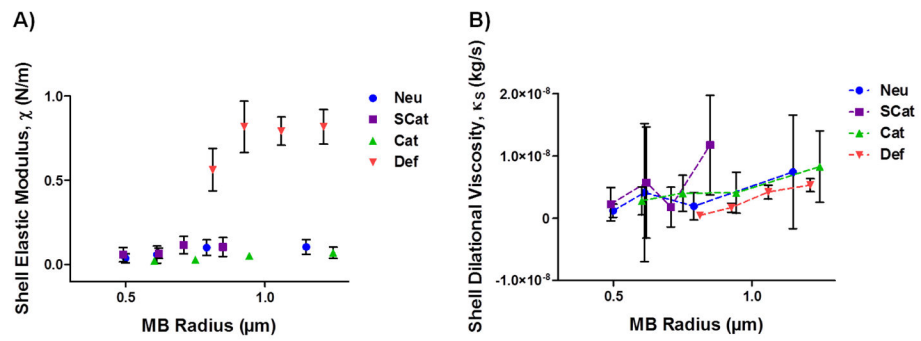
Figure 1.
Acoustic characterization was performed with a modified flow cytometer to determine the shell mechanical properties: **(A)** shell elastic modulus and **(B)** shell dilatational viscosity. Data is presented as mean ± SD.
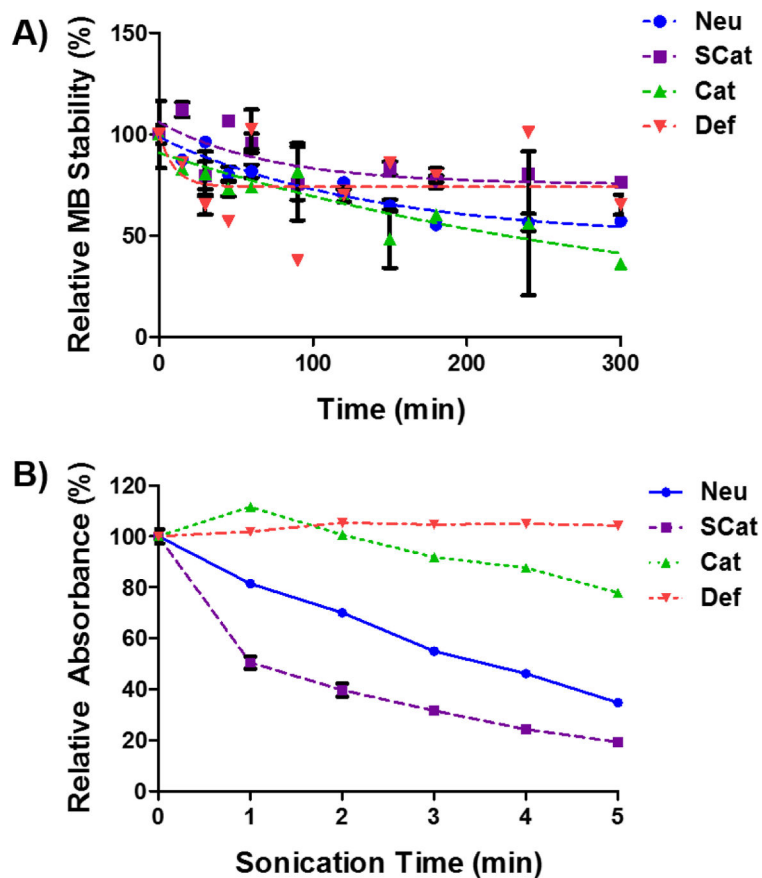
Figure 2.
(A) MB stability over time relative to initial concentration **(B)** Turbidity of MB suspensions as measured by absorbance after US sonication. Data is presented as mean ± SD, n = 3.
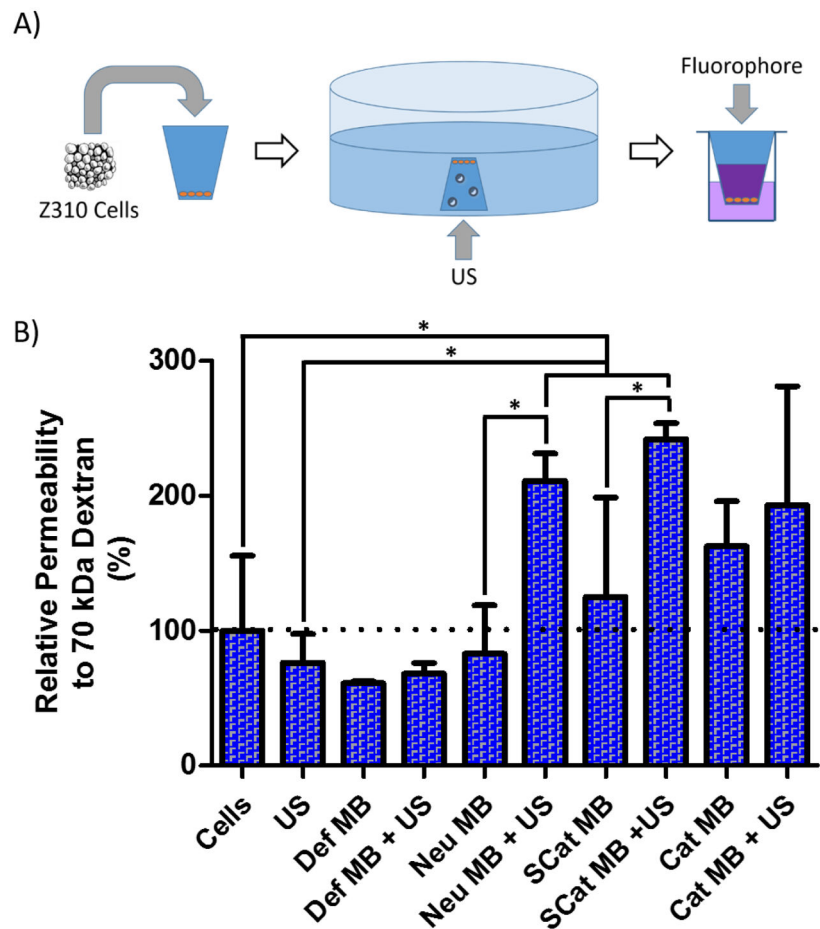
Figure 3.
(A) Schematic of method to determine choroid plexus epithelium permeability to fluorescent polymers after MB sonoporation. Z310 choroid plexus cells were seeded in transwells and allowed to grow into a monolayer. The transwell was submerged in OptiMEM™, exposed to MBs and US, and filled with fluorescent polymers to determine leakage through to the bottom well. **(B)** Permeability of Z310 choroid plexus cell monolayers to 70 kDa Texas Red-dextran after sonoporation with MBs and US. Data is presented as mean + SD, n = 4. Statistically significant ($P < 0.05$) differences are indicated with a (*).
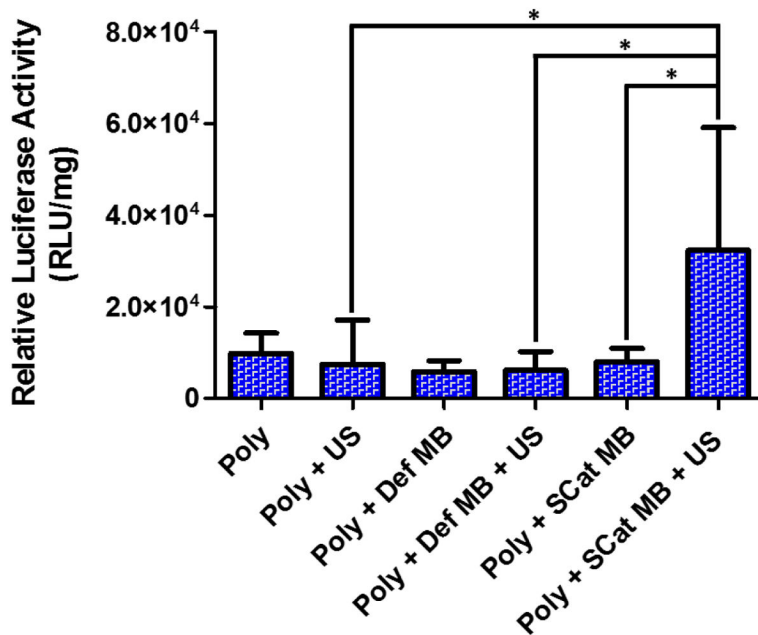
Figure 4.
Luciferase expression in the mouse right brain after treatment with polyplexes, MBs, and US. Data is presented as mean + SD, n = 6 or 9. Statistically significant ($P < 0.05$) differences are indicated with a (*).
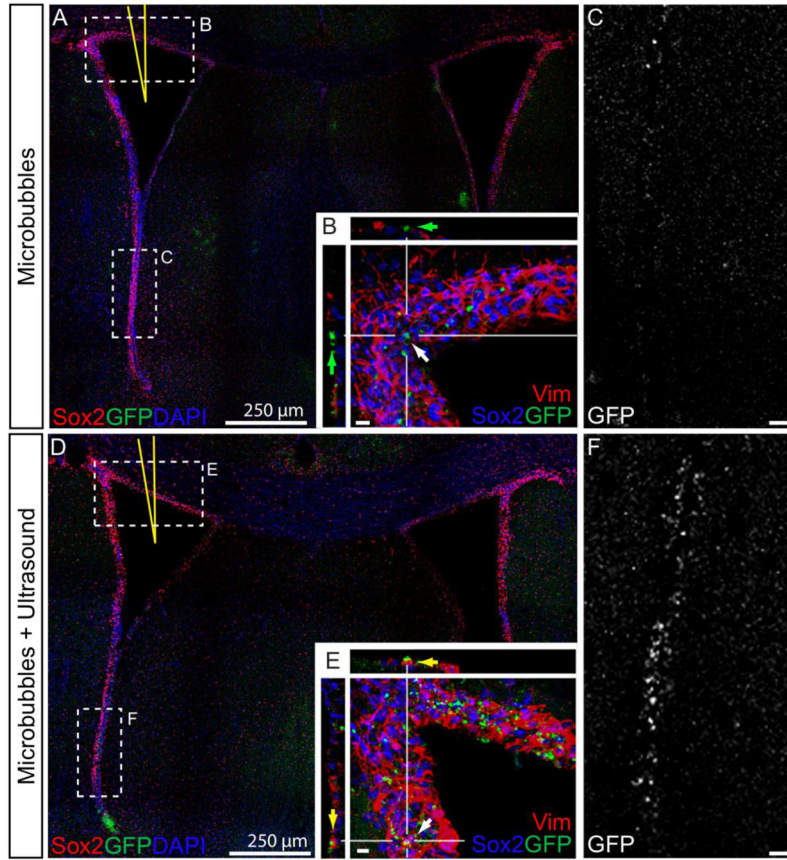
Figure 5.
Confocal micrographs of cells expressing GFP after *in vivo* transfection with SCat MBs. Brains injected with polyplexes and SCat MBs in the lateral ventricle (**A**, yellow needle) showed a lesser number of transfected cells (GFP⁺, Green) along the ependymal cells (vimentin⁺, Red) of the dorsal aspects of the ventricle (**B**) than brains treated with SCat MBs and US (**D** & **E**). Along the ventral walls of the SVZ, more fluorescence is observed in the GFP channel images of brains treated with MBs and US (**F**) than in brains with MBs only (**C**). Small bar, 10 μm.
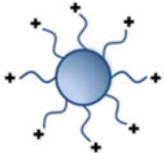
Table 1

Lipid compositions of MBs

MB	Surface Charge	Lipid Composition (mol %)				Schematic
		DSPC	DSPE-mPEG2000	DSPE-PEG2000-Amine	DSTAP	
Neu	Neutral	90	10	—	—	
SCat	Slightly Cationic	90	—	10	—	
Cat	Cationic	70	—	10	20	

Table 2

Physical characterization of MBs

MB	Average Diameter (μm)	Concentration (MB/mL)	Average Zeta Potential (mV)
Neu	1.020 ± 0.270	1.04E+10	−10.6 ± 0.8
SCat	1.021 ± 0.274	1.34E+10	17.0 ± 0.3
Cat	0.958 ± 0.294	8.37E+09	29.8 ± 0.3
Def	1.286 ± 0.765	1.92E+10	−1.1 ± 0.2
Opt	1.644 ± 1.076	4.61E+8	−25.3 ± 2.7